RSC Advances

ROYAL SOCIETY OF CHEMISTRY

www.rsc.org/advances

Synthesis, crystal structure, DNA interaction and *in vitro* anticancer activity of a Cu(II) complex of purpurin: Dual poison for human DNA topoisomerase I and II

Piyal Das[a], Chetan Kumar Jain[b,d], Sanjoy K. Dey[c], Rajat Saha[c], Abhishek Dutta Chowdhury[a], Susanta Roychoudhury[b], Sanjay Kumar[c], Hemanta Kumar Majumder[d] Saurabh Das[*a]

[a] Department of Chemistry, Jadavpur University, Kolkata-700032, India.

[b] Cancer Biology & Inflammatory Disorder Division, Indian Institute of Chemical Biology, Kolkata-700032, India.

[c] Department of Physics, Jadavpur University, Kolkata-700032, India.

[d] Infectious Diseases and Immunology Division, Indian Institute of Chemical Biology, Kolkata-700032, India.

E-mail: sdas@chemistry.jdvu.ac.in (S. Das)
kumars@phys.jdvu.ac.in (S. Kumar)
hkmajumder@iicb.res.in (H. K. Majumder)

Abstract

Although generation of reactive oxygen species (ROS) by anthracycline anticancer drugs is essential for anti-tumor activity they make these drugs cardiotoxic. Metal-anthracyclines that generate relatively fewer ROS are effective antitumor agents. Purpurin (LH_3), a hydroxy-9, 10-anthraquinone, closely resembles doxorubicin, an established anthracycline drug. This molecule was chosen to see the extent to which simpler analogues are effective. A Cu(II) complex of LH_3 [$Cu^{(II)}$-$(LH_2)_2$] was synthesized to mimic the metal-anthracycline complexes. The crystal structure of [$Cu^{(II)}$-$(LH_2)_2$] was determined by Rietveld refinement of PXRD data using an appropriate structural model developed on the basis of spectroscopic data. It is the first report on crystal structure of any hydroxy-9,10-anthraquinone with a 3d-transition metal ion. The bond lengths and bond angles obtained by structural refinement corroborate those calculated by DFT method. DNA binding of the complex was slightly better than purpurin. However, more importantly unlike purpurin, binding constant values did not decrease with increase in pH of the medium. DNA relaxation assays show $Cu^{(II)}$-$(LH_2)_2$ as a novel potent dual inhibitor of human DNA topoisomerase I and topoisomerase II enzymes. $Cu^{(II)}$-$(LH_2)_2$ stabilizes covalent topoisomerase-DNA adducts both *in-vitro* and within cancer cells. The cleavage assay keeps the complex well ahead of LH_3 with regard to efficacy. These results paralleled those of cell growth inhibition and showed that the complex was more effective in killing ALL MOLT-4 cells than LH_3, suggesting it targets topoisomerase enzymes within cells. The NADH dehydrogenase assay revealed further that the generation of superoxide was less in case of the complex compared to LH_3.

Keywords: Anthracyclines, purpurin, Cu(II)-purpurin complex, crystal structure, DNA topoisomerase, ALL MOLT-4 cells, ROS generation, anticancer drug.

1. Introduction

Anthracycline anticancer agents are currently in use in various forms of chemotherapy.[1] The two most well known drugs in this series, adriamycin (doxorubicin, DOX) and daunomycin are extensively used in breast cancer and acute lymphoblastic leukemia (ALL). These compounds function as DNA topoisomerase inhibitors.[1] DNA topoisomerases are essential nuclear enzymes found in cells that help to maintain DNA topology during processes like replication, transcription and recombination, ensuring the faithful segregation of chromosomes during cell division.[1-3] The nucleus of mammalian cells contain two principal types of DNA topoisomerases, DNA topoisomerase I (topo I) and DNA topoisomerase II (topo II) that are molecular targets for several anticancer drugs.[2,3] Topoisomerase inhibitors belong to two different classes. Class I inhibitors or topoisomerase poisons inhibit controlled strand rotation or the re-ligation step of the enzymatic reaction cycle forming enzyme linked DNA lesions that initiate cell cycle arrest leading to apoptosis.[4] Class II inhibitors or catalytic topoisomerase inhibitors inhibit DNA binding or the DNA nicking step of the enzyme-reaction cycle.[5-8]

The major concern on the use of anthracyclines is their associated cardiotoxicity and life-threatening heart damage.[9-18] Studies on breast cancer itself reveal, ~27% of the patients suffer congestive heart failure later in life owing to anthracycline treatment.[19, 20] Reports have indicated reactive oxygen species (ROS) produced by anthracyclines are mainly responsible for cardiotoxicity and that the hydroxy-9,10-anthraquinone moiety present in these molecules is the seat of generation of ROS.[1] At the same time, ROS is essential for anticancer activity also.[21, 22] Hence, there is a need to have a proper balance in the generation of ROS such that it maintains anticancer activity but is not cardiotoxic. Lowering ROS generation to appropriate levels could be one approach to minimize side effects of these drugs and their analogues.

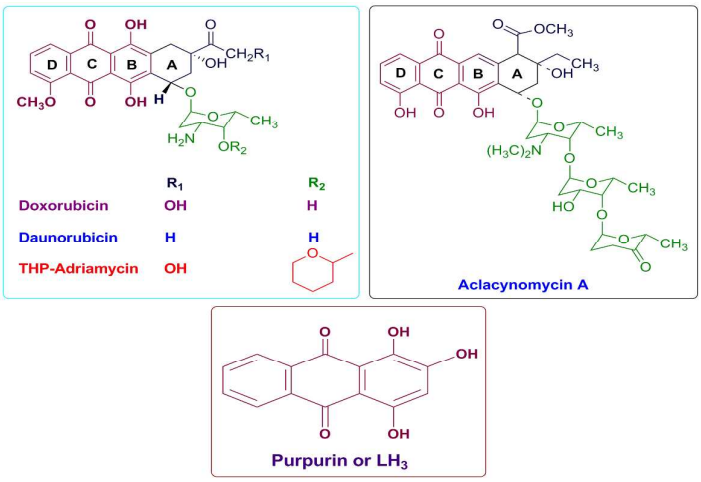

Recent studies on hydroxy-9,10-anthraquinones and their metal complexes have shown remarkable similarity with anthracyclines particularly with regard to physicochemical attributes, electrochemical behavior and biophysical interactions.[23-25] Cardiotoxicity of anthracyclines was shown to decrease significantly when they form complexes with metal ions.[26,27] Complexes of Cu(II) with anthracyclines generate relatively less ROS but are effective anti-cancer agents.[26-29] With these facts in mind, our aim was to pick simple hydroxy-9,10-anthraquinones, prepare their complexes and compare them with similar complexes of anthracyclines.[30] Purpurin (1, 2, 4-trihydroxy-9, 10-anthraquinone) that closely resembles DOX was chosen and a Cu(II) complex was prepared. Results obtained with this complex was compared with Cu(II) complexes of DOX with regard to semiquinone formation, DNA interaction, action on DNA topoisomerase enzymes to realize its potential as an anticancer agent.[31]

2. Experimental

2.1 Synthesis of a Cu(II) complex of LH_3

Purpurin (LH_3) of ~96% purity was purchased from Sigma-Aldrich and further purified by re-crystallization from ethanol-water mixtures. The compound being photosensitive, was

stored in the dark. The complex was prepared by mixing $Cu(NO_3)_2.3H_2O$ and LH_3 in the ratio 1:2 (metal to ligand stoichiometry determined by mole-ratio method, Supplementary section). LH_3 (0.09 mmol) and $Cu(NO_3)_2.3H_2O$ (0.045 mmol) were dissolved in a minimum volume of hot absolute ethanol and triple distilled water respectively. The Cu(II) solution was added drop by drop to the yellowish-orange solution of LH_3 taken in a beaker, with continuous stirring with the help of a temperature controlled magnetic stirrer. The intense yellowish-orange color of LH_3 changed almost immediately to dark brown upon addition of the aqueous Cu(II) solution. Solvent ratio was 2:1 ethanol-water. The reaction mixture was stirred for 2 hours at 40˚C. After 2 hours, it was kept overnight in the dark. A brown colored solid settled to the bottom of the beaker while the supernatant was yellow in color. The solution was filtered. The brown residue was washed with warm 10% ethanol solution. It was then purified from acetonitrile and dried in a vacuum desiccator. Utmost care was taken to prevent the formation of a polymeric 1:1 complex under alkaline conditions.[32] pH of the medium was maintained at ~ 6.00 using sodium bicarbonate.

Yield: 68 %. Analytical calculation (%) for $CuC_{28}H_{18}O_{12}$: C, 55.13; H, 2.95. Experimentally found: C, 54.81; H, 2.90. Cu(II) was estimated using standard procedure.[33] Analytical calculation (%) 10.42, experimentally found 10.34. UV-Vis spectra: λ_{max} at 515 nm. MS (m/z): 630 $[M + Na]^+$.

2.2 X-ray powder diffraction measurements and crystal structure of $Cu^{(II)}$-$(LH_2)_2$

The X-ray powder diffraction data was collected on Bruker D8 Advanced powder diffractometer using CuKα radiation (λ=1.5418 Å). The generator settings were 40kV and 40mA. Diffraction pattern was recorded at room temperature (21°C) with step size 0.0199^o (2θ) and a count time of 5 sec per step over the 2θ range of 5°-80°. The X-ray powder diffraction pattern was indexed by NTREOR of EXPO 2009 package and results indicate the sample crystallizes in a triclinic unit cell with a =12.575 Å, b =12.412 Å, c =10.343 Å

and α=97.09°, β=113.49°, γ=62.38° [M(20) = 14, F(20) = 14.(0.003767, 338)].[34] The statistical analysis of powder patterns using the FINDSPACE of EXPO 2009 software package indicates that the most probable space group is *P-1*. Structure was solved by global optimization method in direct-space using Monte Carlo based simulated annealing technique (in parallel tempering mode) as implemented in the program FOX with the help of an initial structural model developed on the basis of spectroscopic information (provided in "Supplementary Information").[35] The initial molecular geometry was optimized by MOPAC 2007 program and this optimized structural model was used as an input to the FOX program in order to obtain the atomic coordinates.[35, 36] The atomic coordinates thus obtained from FOX were used as the starting model for Rietveld refinement carried out by the GSAS software package with EXPGUI interface.[37, 38] The lattice parameters, background coefficients and profile parameters were refined. The background was described by the shifted Chebyshev function of the first kind with 24 points regularly distributed over the entire 2θ range. A fixed isotropic displacement parameter of 0.04 $Å^2$ for all non-hydrogen atoms and 0.06 $Å^2$ for hydrogen atoms was maintained. In the final stage of refinement, preferred orientation correction was applied using the generalized spherical harmonic model of order 10.

2.3 Computational Details

Full geometry optimizations were carried out at the (U)B3LYP levels using density functional theory method with Gaussian 09 (revision A.02).[39-41] All elements were assigned by the LanL2DZ basis set with effective core potential.[42, 43] Stationary-point calculations were carried out using the output coordinates from the geometry optimization calculations. GaussSum was used to calculate fractional contributions of various groups to each molecular orbital.[44, 45] No symmetry constraints were imposed during structural optimizations and the nature of the optimized structures and energy minima were defined

by subsequent frequency calculations. Natural bond orbital analyses were performed using NBO 3.1 module of Gaussian 09 on optimized geometry.[46-49] All calculated structures were visualized with ChemCraft.[50]

2.4 Electrochemistry of $Cu^{(II)}$-$(LH_2)_2$

Cyclic voltammetry was performed on an EG & G Potentiostat Model 263A, Princeton Applied Research having power suite software for electrochemistry. Voltammograms were recorded using the three-electrode system. A glassy-carbon electrode of surface area 0.1256 cm^2 was the working electrode, Ag/AgCl, KCl (saturated) was the reference while a platinum wire served as the counter electrode. Electrochemical measurements were done in a 50 ml electrochemical cell with dimethyl formamide (DMF) as the solvent and 0.1 (M) tetrabutylammonium bromide (TBAB) as supporting electrolyte.[23, 24] Before each cyclic voltammetry experiment, the solution was purged using high purity Argon for 40 minutes while in between each scan the solution was purged with Argon for a further 5 minutes.

2.5 Interaction of LH_3 and $Cu^{(II)}$-$(LH_2)_2$ with CT DNA

2.5.1 By UV-Vis spectroscopy

Interaction was studied using a JASCO V-630 UV-Vis spectrophotometer. A pair of quartz cuvettes (STARNA Scientific Ltd.; 10mm×10mm path length) was used. Separate aliquots, each containing a constant concentration (75 μM) of LH_3 or $Cu^{(II)}$-$(LH_2)_2$ and different concentrations of CT DNA were used at different pH. CT DNA was gradually increased until saturation was reached. The total volume was kept constant at 2.0 ml using 15 mM Tris buffer and 120 mM NaCl. At the end of the titration, CT DNA was ~30 folds greater than the concentration of compounds used. Each experiment was repeated thrice.

Binding constant and site size of interaction was determined using standard equations.[23, 24, 33, 51, 52]

2.5.2 By fluorescence spectroscopy

Interaction was studied using a HITACHI S-7000 fluorescence spectrophotometer.[23, 24, 32] Solutions were excited at 515 nm and emission was measured at 582 nm at 298 K. The complex (75 μM) was taken in a fluorescence cuvette (10mm×10mm path length) and titrated with increasing amounts of CT DNA. The total volume (2.0 ml) was constant using 15 mM Tris buffer (pH 7.4) and 120 mM NaCl. Here too, at the point of saturation, CT DNA was ~30 folds greater than the concentration of $Cu^{(II)}$-$(LH_2)_2$. The experiment was repeated thrice. Binding constant and site size of interaction was evaluated.

2.6 DNA relaxation assays for topoisomerase I and topoisomerase II enzymes

Recombinant human DNA topoisomerase I and human DNA topoisomerase II enzymes were purchased from TopoGEN Inc (Port Orange, Florida, USA). DNA relaxation assays for recombinant human DNA topoisomerase I and topoisomerase II enzymes were performed in the presence and absence of the compounds by briefly incubating 100 fmol of supercoiled pBS SK (+) DNA with 50 fmol of the enzyme in the reaction buffer provided with the enzymes. Dimethyl sulphoxide (DMSO) concentration was maintained at 1% (vehicle control). Camptothecin (CPT) and Doxorubicin (DOX) were purchased from Sigma (St. Louis, MO, US) to be used as positive control drugs that stabilize covalent topoisomerase I-DNA complexes and covalent topoisomerase II-DNA complexes respectively. Reactions were incubated at 37°C for 30 minutes, loaded on 1% agarose gel and electrophoresed at 20 volts overnight. After completion of electrophoresis, gels were stained with 0.5 μg/ml ethidium bromide and viewed by Gel Doc 2000 (BioRad) under UV illumination. Relaxation was assessed by monitoring the decreased electrophoretic mobility of relaxed topoisomers of pBS SK (+) DNA.

2.7 DNA cleavage assay for topoisomerase I and topoisomerase II enzymes

DNA cleavage assay for topoismerase I and topoismerase II was performed in the presence or absence of the compounds by briefly incubating 100 fmol of supercoiled pBS (SK^+) DNA with 500 fmol of enzyme. For topoisomerase I, the reaction buffer contained 10 mM Tris-HCl (pH 7.5), 50 mM KCl, 5 mM $MgCl_2$, 0.1 mM EDTA and 15 µg/ml BSA while for topoisomerase II, assay was done in 1X mixture of the two reaction buffers provided with the enzyme. All reactions were performed in the presence of 400 µM N-acetyl cysteine (NAC) (Sigma) and 100 µM ascorbic acid (AA) (Sigma). Reactions were incubated at 37 ^oC for 30 minutes and stopped with 0.5% SDS. Enzymes were digested by proteinase K treatment. DMSO concentration was maintained at 1% (vehicle control). CPT and DOX were used as positive control drugs that stabilize covalent topoisomerase I-DNA complexes and covalent topoisomerase II-DNA complexes respectively. Reactions were loaded on 1% agarose gel with 0.5 µg/ml ethidium bromide. Electrophoresis at 80 volts was done for 3 hours. After completion of electrophoresis, gels were viewed by Gel Doc 2000 (BioRad) under UV illumination.

2.8 Cell culture and cell viability assay

MOLT-4 cells were cultured in RPMI medium (GIBCO, Invitrogen, Carlsbad, CA, US), supplemented with 10% fetal bovine serum (GIBCO), antibiotic mixture (1X) PSN (GIBCO) and gentamicin reagent solution (GIBCO). Cells were incubated in a humidified CO_2 incubator at 37°C. Etoposide (ETO) was purchased from Sigma (St. Louis, MO, US) to be used as a positive control drug along with CPT and DOX. These were dissolved in DMSO. MOLT-4 cells were seeded in 96 well plates for 24 hours before drug treatment. After 24 hours, cells were treated with LH_3, $Cu^{(II)}$-$(LH_2)_2$ and the control compounds. DMSO concentration was less than 0.5%. After treatment for 72 hours cell viability was checked by 3-(4,5-dimethylthiazol-2-yl)-2,5-diphenyltetrazolium bromide (MTT) assay.

Briefly, cells were washed with 1X PBS and treated with MTT for 4 hours at 37°C. Precipitates were dissolved in DMSO and plates were analyzed on Thermo MULTISKAN EX plate reader at 595 nm.

2.9 Immunoband depletion assay

For the immunoband depletion assay MOLT-4 cells were cultured in 35 mm dishes and treated with either 10 μM CPT or 10 μM DOX or 40 μM LH_3 or 20 μM $Cu^{(II)}$-$(LH_2)_2$. Cells were harvested at 0 hour, 4 hours, 8 hours and 12 hours time points. Equal amounts of protein were electrophoresed on SDS-poly acryl amide gel. Separated proteins were then transferred on to a nitrocellulose membrane and western blotting was performed using anti-topo I and anti-topo II antibodies (Santa Cruz Biotechnology, Inc. Santa Cruz, CA, USA).

2.10 NADH dehydrogenase assay

The enzyme assay was done at 298 K with cytochrome c as electron acceptor.[25, 53] LH_3 and $Cu^{(II)}$-$(LH_2)_2$ were assayed for NADH-cytochrome c reductase activity monitoring the reduction of cytochrome c at 550 nm. Tris buffer (pH ~7.4), 80.0 μM cytochrome c, 160.0 μM NADH, 3.0 U/lit NADH dehydrogenase and test compounds were used. LH_3 and $Cu^{(II)}$-$(LH_2)_2$ concentrations were varied from 0 to 45.0 μM. Activity of NADH dehydrogenase is expressed in units where one unit of activity reduces 1.0 μ mole oxidized cytochrome c per minute at 298 K. Formation of superoxide radical anion catalyzed by LH_3 and $Cu^{(II)}$-$(LH_2)_2$ was measured from the reduction of cytochrome c inhibited by superoxide dismutase (SOD) (0 or 40.0 μg/ml) in the presence of NADH and NADH dehydrogenase.[25-27] The kinetics software of JASCO V-630 was utilized for the purpose.

3. Results and Discussions

3.1 X-ray crystal structure description of [$C_{28}H_{14}O_{10}$ Cu]

Structural analysis from PXRD data (Fig.1a) indicates that the Cu(II) complex crystallizes in *P-1* space group. The ORTEP diagram for the complex is depicted in Fig. 1b. According to the refined structure obtained by analyzing the PXRD data each asymmetric unit of the complex contains one Cu(II) ion, two monanionic LH_2^- units and two guest water molecules. Each Cu(II) center shows perfect square planar geometry with coordination number four. The coordination environment of Cu(II) is satisfied by two deprotonated phenolic –OH groups (O18 and O35) of two different LH_3 units and two carbonyl oxygen atoms (O19 and O34). The crystal structure obtained by Rietveld refinement of PXRD data exhibits that all Cu-O bond distances vary in the range 1.847-1.884 Å and all *cisoid* and *transoid* angles vary in the range 87.2^o-92.9^o and 179.86^o-179.89^o respectively. Two LH_3 units are inversely connected to the metal center; each monomeric unit is connected by supramolecular interactions leading to higher dimension. The ORTEP diagram of the $Cu^{(II)}$-$(LH_2)_2$ complex (Fig. 1b) almost completely matches the DFT optimized structure (Fig. 1c). In the absence of a single crystal for systems such as this one, powder X-ray diffraction remains the only option to obtain a structure. In our case, the structure obtained from powder diffraction not only matched other experimental findings but also was in good agreement with DFT calculations. This is the first reported structure of a complex of any hydroxy-9, 10-anthraquinone with a 3d-transition metal ion.[30] Final crystallographic data, structure refinement parameters, selected bond length and bond angles are summarized in Table 1 and Table 2.

3.2 DFT study of $Cu^{(II)}$-$(LH_2)_2$ complex

Although the structure of $Cu^{(II)}$-$(LH_2)_2$ was obtained from powder X-ray diffraction data, a DFT study was done to check the formation of the complex and to predict certain physical and chemical properties. The MO composition of $Cu^{(II)}$-$(LH_2)_2$ from DFT calculations is provided in Table 1S. The α-HOMOs and β-LUMOs are primarily composed of redox

non-innocent quinone moieties of $Cu^{(II)}$-$(LH_2)_2$ that essentially make the paramagnetic copper centre a redox silent site [Fig. 1d-1g]. DFT calculations of $Cu^{(II)}$-$(LH_2)_2$ predict quinone based redox processes. Analysis of the spin density plot (Fig. 1h) predicts a mixed metal-ligand behavior of the paramagnetic copper center that was experimentally verified in the EPR spectrum of the complex (supplementary section). The TDDFT calculation revealed electronic transitions obtained in the UV-Vis spectrum would be LLCT (Table 3). DFT computer predictions of $Cu^{(II)}$-$(LH_2)_2$ were in excellent agreement with the solved structure with calculated bond lengths and angles being very close to that obtained through a computer model that provided a best fit for the experimental data (Fig. 1b, 1c and Table 1, 2).

3.3 Electrochemical behavior of $Cu^{(II)}$-$(LH_2)_2$ complex

The complex showed one-electron reduction in DMF (Fig. 2a) with a peak at -0.866 V (*vs.* Ag,AgCl/ KCl saturated) and $E_{1/2}$ = -0.810 V was similar to an earlier report from our laboratory.[32] In case of LH_3, we reported earlier that the molecule undergoes two-step one-electron reduction forming a semiquinone that converts to a quinone di-anion.[23] The variation of cathodic peak current with square root of potential sweep rate according to Randles equation (Eq. 1) was linear in case of the complex (Fig. 2b) indicating reduction of $Cu^{(II)}$-$(LH_2)_2$ in DMF was diffusion controlled.[55, 56]

$$i_{pc} = (2.69 \times 10^5).\ n^{3/2}.\ D_0^{1/2}.\ A.\ C.\ \nu^{1/2} \qquad (1)$$

i_{pc} = cathodic peak current (A), n = total number of electrons involved, A = area of the electrode (cm^2), C = concentration ($moles/cm^3$), ν = scan rate (V/s). The diffusion coefficient (D_0) was calculated from the slope of the plot (Fig. 2b) and found to be 4.462×10^{-5} cm^2/s. The ratio of peak currents at different potential sweep rates were calculated with the help of Nicholson's equation.[56, 57]

$$i_{pa}/i_{pc} = \frac{(i_{pa})_0}{i_{pc}} + \frac{0.485 \times (i_{sp})_0}{i_{pc}} + 0.086 \quad (2)$$

$(i_{sp})_0$ was the current at E_λ (switching potential) and $(i_{pa})_0$ was the uncorrected anodic peak current with respect to zero current (baseline). The experimental data in Table 4 shows ratio of peak currents (i_{pa}/i_{pc}) was unity at all scan rates. This indicates that the redox behavior of $Cu^{(II)}$-$(LH_2)_2$ in an aprotic solvent like DMF was completely reversible. Redox processes of the complex obtained from cyclic voltammetry studies corroborate the prediction made earlier from DFT calculations that redox processes would be quinone based. The Cu(II)/Cu(I) couple had a reduction potential of 0.55 V vs. Ag,AgCl/ KCl (saturated) in acetonitrile solvent.

3.4 Interaction of LH_3 with CT DNA by UV-Vis spectroscopy: The effect of pH

A detailed study on the interaction of LH_3 with CT DNA was reported earlier.[23] In that report, we showed that LH_3 is a DNA intercalator. Intrinsic binding constant and site size of interaction was found to be $(4.51 \pm 0.20) \times 10^4$ M^{-1} and (5.21 ± 0.20) nucleotides respectively.[23] In this study, an effort was made to show the manner in which the intrinsic binding constant for the interaction of LH_3 with DNA varied with pH at constant ionic strength of the medium. It was observed as pH increased the extent of interaction between LH_3 and CT DNA decreased (Table 2S) attributed to the generation of an anionic form of LH_3 at physiological pH.[58] With increase in pH, LH_2^- formed from LH_3 faced more repulsion from DNA that manifested by a decrease in binding constant values. Since LH_3 exists in two forms at physiological pH [6.65 to 8.35], hence binding of it to CT DNA at any pH in the specified range was a consequence of both.[58] To know the contribution of each and the impact that a change in pH has on the strength of interaction, the overall

binding constant at each pH was treated according to the Henderson-Haselbach equation (Equation 3).[58, 59]

$$pH = pK_a + \log \frac{[D^-]}{[D_0]} \qquad (3)$$

Impact of the negative charge on LH_2^- on the overall binding constant was determined by plotting K^* at five different pH values. Thus, the contribution of each form towards overall binding constant was evaluated with the help of equations 8 & 9. The overall binding constant could be defined as

$$K^* = \frac{[C_b]}{[C_f]\,[DNA]} \qquad (4)$$

The change in absorbance of LH_3 upon binding enabled the determination of C_b and C_f (supplementary section). [DNA] represents the total concentration of CT DNA. Since overall binding constant at each pH was considered to be made up of two terms K^0 and K^-, hence K^0 was defined as the overall binding constant of the neutral form ($K^0 = \frac{[C_b{}^0]}{[C_f{}^0][DNA]}$) while K^- was that due to the anionic form ($K^- = \frac{[C_b{}^-]}{[C_f{}^-][DNA]}$). The total bound and free forms of purpurin were

$$[C_b] = [C_b{}^0] + [C_b{}^-] \qquad (5)$$

and $$[C_f] = [C_f{}^0] + [C_f{}^{--}] \qquad (6)$$

$$pH = pKa + \log \frac{[C_f{}^-]}{[C_f{}^0]} \qquad (7)$$

Equation 4 could then be written as

$$K^* (1 + 10^{pH - pK}) = K^0 + K^- \times 10^{pH - pK} \qquad (8)$$

Or

$$K^* = (K^0 + K^- \times 10^{pH - pK})/(1 + 10^{pH - pK}) \qquad (9)$$

According to equation 8, plot of $K^*(1 + 10^{pH - pK})$ as a function of $10^{pH - pK}$ yields a straight line (Fig. 3a) with a correlation coefficient 0.99. K^- was determined as the slope

and K^0 as the intercept. Values were (5.65 ± 0.48) × 10^6 M^{-1} and (2.41 ± 0.04) × 10^4 M^{-1} for K^0 and K^- respectively. Overall binding constants (K^*) were also plotted against pH according to equation 9 (Fig. 3b) and values for K^0 and K^- were (4.61 ± 0.10) × 10^6 M^{-1} and (2.69 ± 0.07) × 10^4 M^{-1} respectively. Knowing the contributions of the neutral (K^0) and mono-anionic (K^-) forms of purpurin, one is now in a position to calculate K* for purpurin binding to CT DNA at any pH. Results indicate the negative charge on the anionic form of LH_3 (LH_2^-) holds the molecule back from interacting with CT DNA that might have an impact on its overall potency.[58, 60] If the generation of the negative charge on LH_3 is prevented then the overall binding constant (K*) should increase allowing purpurin to have binding constants with CT DNA that are comparable to those reported for anthracyclines.[59] This is expected from a structure-function correlation that is today an important feature in understanding modern aspects in chemical biology.[60]

3.5 Interaction of $Cu^{(II)}$-$(LH_2)_2$ with CT DNA

3.5.1 By UV-Vis spectroscopy

$Cu^{(II)}$-$(LH_2)_2$ has a peak at 515 nm at physiological pH that gradually decreased in intensity on adding CT DNA. The spectra also showed a slight blue shift by 4-7 nm (Fig. 3c). Interaction between the electronic states of the $Cu^{(II)}$-$(LH_2)_2$ chromophore and those of the DNA bases could be a reason for this hypsochromic shift.[23, 24] These spectral features suggest interaction between $Cu^{(II)}$-$(LH_2)_2$ and CT DNA was a case of intercalation through an ordered stacking of $Cu^{(II)}$-$(LH_2)_2$ between aromatic heterocyclic base pairs of the DNA helix.[23, 24, 32] л-л stacking and dipole-dipole interactions help to stabilize the [$Cu^{(II)}$-$(LH_2)_2$]-DNA adduct formed as a consequence of interaction between the electron-deficient quinones of $Cu^{(II)}$-$(LH_2)_2$ and electron-rich purine or pyrimidine bases of the DNA helix.[24]

Overall binding constant (K*) was determined with the help of standard equations (supplementary section) [shown in Figs. 3d, S7(a), S7(b)]. Results are summarized in Table 5. Under condition of 1:1 compound-DNA adduct formation, presence of excess CT DNA compared to $Cu^{(II)}$-$(LH_2)_2$, the Benesi-Hildebrand equation (Eq. 10) was used to determine K^*.[23, 24, 61]

$$\frac{A_0}{A-A_0} = \frac{\epsilon_G}{\epsilon_{H-G}-\epsilon_G} + \frac{\epsilon_G}{\epsilon_{H-G}-\epsilon_G}\cdot\frac{1}{K'[DNA]} \qquad (10)$$

A_0 and A are absorbances of $Cu^{(II)}$-$(LH_2)_2$ in the absence and presence of CT DNA; ϵ_G and ϵ_{H-G} are absorption coefficients of $Cu^{(II)}$-$(LH_2)_2$ and its adduct with DNA respectively. The plot of $A_0/(A-A_0)$ versus 1/[DNA] [Fig. S7(c)] was linear. K* is reported in Table 5.

Upon complex formation, dissociation of the phenolic-OH at C_2 of LH_3 is retarded with its pK value now being well beyond the physiological pH. As a result, formation of anionic species for $Cu^{(II)}$-$(LH_2)_2$ did not arise and we found at all pH values (in the physiological pH range) the complex not only had a higher binding constant compared to purpurin (LH_3) but more importantly the values remained constant over a considerable pH range.[60] This aspect has a lot of significance for cancer patients for whom there occurs fluctuations in body pH.

3.5.2 By fluorescence spectroscopy

Interaction of $Cu^{(II)}$-$(LH_2)_2$ with CT DNA was followed at physiological pH by monitoring the increase in fluorescence upon adding CT DNA to a constant concentration of $Cu^{(II)}$-$(LH_2)_2$. An increase in fluorescence was an indication that the mode of interaction was intercalation as observed earlier for LH_3.[23] The emission spectrum of $Cu^{(II)}$-$(LH_2)_2$ (Fig. 3e) exhibited a maxima at 582 nm that was used to calculate the change in fluorescence (ΔF). Binding parameters for $Cu^{(II)}$-$(LH_2)_2$ with CT DNA were analyzed using the same

equations as mentioned for the UV-Vis study. For the purpose of analysis, the change in fluorescence intensity (ΔF) was considered instead of ΔA (equations are provided in the supplementary section). In case of fluorescence, our approach was based on the assumption that fluorescence intensity was linearly proportional to the concentration of $Cu^{(II)}$-$(LH_2)_2$ bound to CT DNA. ΔF_{max} and K_{app} (= K_d^{-1}) were obtained from typical double reciprocal plots as the intercept and slope respectively [Fig. S8(a)]. $\Delta F/\Delta F_{max}$ was plotted against concentration of CT DNA. Applying non-linear fitting K_{app} (= K_d^{-1}) was obtained (Fig. 3f). Data obtained from fluorimetric titration of $Cu^{(II)}$-$(LH_2)_2$ with CT DNA was also analyzed according to Scatchard [Fig. S8(b)].[61] Results are summarized in Table 5. The data obtained from fluorescence and UV-Vis studies corroborate each other.

3.6 In-vitro activity of LH_3 and $Cu^{(II)}$-$(LH_2)_2$ on human topoisomerase enzymes

To check inhibitory effects of LH_3 and $Cu^{(II)}$-$(LH_2)_2$ on human DNA topoisomerase I and human DNA topoisomerase II, DNA relaxation assays were performed using recombinant human DNA topoisomerase enzymes in the absence and presence of the compounds (Materials and Methods). Relaxation assay is based on the fact supercoiled DNA molecules are relaxed by active topoisomerase enzymes resulting in the formation of topoisomers of relaxed DNA molecules. These topoisomers migrate slowly compared to supercoiled plasmid DNA in agarose gel. Therefore, the activity of the enzymes may be checked by observing the gel bands for relaxed topoisomers. However, when the enzyme gets inhibited, bands for the relaxed topoisomers do not appear on the gel. We found $Cu^{(II)}$-$(LH_2)_2$ completely inhibited DNA topoisomerase I and DNA topoisomerase II relaxation activities at a concentration of 20 μM while LH_3 had no effect at this concentration (Fig. 4a and 4b). We used established positive control inhibitors, CPT and DOX for topoisomerase I and topoisomerase II enzymes respectively. kDNA decatenation assay was done for DNA topoisomerase II enzyme in the presence of LH_3 and $Cu^{(II)}$-

$(LH_2)_2$. $Cu^{(II)}$-$(LH_2)_2$ inhibited decatenation activity of DNA topoisomerase II enzyme at 20 μM while LH_3 had no effect at this concentration (Fig. S9). Therefore, our results suggest $Cu^{(II)}$-$(LH_2)_2$ is a novel potent dual inhibitor of topoisomerase I and topoisomerase II enzymes *in-vitro* similar to CPT and DOX. Thus $Cu^{(II)}$-$(LH_2)_2$ inhibit relaxation as well as decatenation activities of topoisomerase II enzymes.

3.7 In vitro stabilization of covalent cleavage complexes by LH_3 and $Cu^{(II)}$-$(LH_2)_2$

In order to find out the type of topoisomerase inhibitor the complex is, plasmid cleavage assays were performed for topoisomerase I and topoisomerase II enzymes as described in Materials and Methods. A plasmid cleavage assay is based on the stabilization of covalent complexes between the enzyme and DNA that decreases mobility of DNA in agarose gel. This is because during complex formation DNA gets nicked and nicked plasmid DNA has lower electrophoretic mobility than supercoiled plasmid DNA. Therefore, when an inhibitor is of type class I it would stabilize covalent complexes that could be observed on agarose gel. The concentration of LH_3 used was double (i.e. 40 μM) that of the complex [$Cu^{(II)}$-$(LH_2)_2$] (20 μM) in order to confirm the fact that the effect was due to the complex as a whole and not due to free ligand. $Cu^{(II)}$-$(LH_2)_2$ stabilized the covalent enzyme-DNA complexes at 20 μM while LH_3 had no effect on such complex formation even when used at 40 μM. CPT that stabilizes covalent topoisomerase I-DNA complexes was used as positive control (Fig. 5a). We further checked the effect of LH_3 and $Cu^{(II)}$-$(LH_2)_2$ on topoisomerase II-DNA covalent complex formation and found $Cu^{(II)}$-$(LH_2)_2$ completely stabilized covalent topoisomerase II-DNA complex at 20 μM while LH_3 had no effect even when used at 40 μM. DOX was used as the positive control drug since it is known to stabilize covalent topoisomerase II-DNA complexes (Fig. 5b). Since $Cu^{(II)}$-$(LH_2)_2$ generates ROS (although insignificant, discussed later), this could be responsible for DNA cleavage also. For this reason, cleavage assays were performed in the presence of NAC

and AA that are well-recognized ROS scavengers.[63, 64] With this result, one can now say that DNA cleavage was due to topoisomerase enzyme inactivation and not due to ROS generation (Fig. 5a, 5b). Together the results are interesting and allow us to speculate $Cu^{(II)}$-$(LH_2)_2$ is a novel poison (class I inhibitor) for topoisomerase I and topoisomerase II enzymes.

3.8 Effect of LH_3 and Cu(II)-$(LH_2)_2$ on viability of MOLT-4 cells

Since DOX and other topo II inhibitors like etoposide (ETO) are used in the treatment of ALL we checked the effects of LH_3 and $Cu^{(II)}$-$(LH_2)_2$ on acute lymphoblastic leukemia (ALL) MOLT-4 cells. MTT assays were performed with CPT (IC_{50} = 8.89 ± 0.19 μM), ETO (IC_{50} = 5.59 ± 0.23 μM) and DOX (IC_{50} = 5.25 ± 0.55 μM) (Fig. 6a). Same cell viability assay was also done for LH_3 and $Cu^{(II)}$-$(LH_2)_2$ on ALL MOLT-4 cells. We found $Cu^{(II)}$-$(LH_2)_2$ kills MOLT-4 cells with an IC_{50} value of 18.59 ± 0.77 μM while the same for LH_3 was 26.35 ± 0.31 μM suggesting $Cu^{(II)}$-$(LH_2)_2$ was more potent than LH_3 (Fig. 6b). We suspect enhanced cell killing by $Cu^{(II)}$-$(LH_2)_2$ was due to inhibition of the human DNA topoisomerase I and topoisomerase II enzymes present in the nucleus of MOLT-4 cells. Although IC_{50} for $Cu^{(II)}$-$(LH_2)_2$ in MOLT-4 cells was higher compared to CPT, ETO and DOX since $Cu^{(II)}$-$(LH_2)_2$ produces relatively low ROS and exerts a novel dual inhibitory action on topoisomerase enzymes it could be developed as a useful as well as a less costly alternative.

3.9 Intracellular stabilization of topoisomerase-DNA covalent complexes by $Cu^{(II)}$-$(LH_2)_2$

To check for intracellular stability of $Cu^{(II)}$-$(LH_2)_2$ and formation of intracellular enzyme-DNA complexes we performed topoisomerase I and topoisomerase II immunoband depletion assay (IDA). IDA is based on the fact if a topoisomerase inhibitor stabilizes the covalent enzyme-DNA complex inside the cell then enzyme molecules become associated

with chromatin and will not be detected in the immunoband of the enzyme. In such a situation, the immunoband for topoisomerases will be depleted in a time dependent manner. Our results for topoisomerase I and topoisomerase II immunoband depletion assays (Fig. 6c) clearly showed $Cu^{(II)}$-$(LH_2)_2$ efficiently depletes the immunoband of both topoisomerase I and topoisomerase II after 12 hour treatment with 20 μM of $Cu^{(II)}$-$(LH_2)_2$. On the contrary, LH_3 did not deplete the immunoband after a similar 12 hour treatment with 40 μM (concentration of LH_3 used was double that of $Cu^{(II)}$-$(LH_2)_2$ in order to confirm that the effect was due to the complex and not free ligand). These results indirectly indicate $Cu^{(II)}$-$(LH_2)_2$ is stable inside the cellular environment and shows without any doubt that it efficiently inhibits topoisomerase I and topoisomerase II enzymes by stabilizing covalent enzyme-DNA complexes.

3.10 NADH dehydrogenase assay of LH_3 and $Cu^{(II)}$-$(LH_2)_2$

Several studies have suggested that the aspect of cardiotoxicity associated with anthracycline anticancer drugs is related to the formation of reduced oxygen species like the superoxide radical anion.[1,10,11,16-18,26,27] It was shown earlier metal complexes of anthracyclines generate less superoxide but are effective against tumors.[27] Keeping this in mind, we compared the generation of superoxide by LH_3 and $Cu^{(II)}$-$(LH_2)_2$ by measuring the reduction of cytochrome c inhibited by superoxide dismutase (SOD).[53] We found increasing the concentration of LH_3, the yield of $O_2^{-\cdot}$ increased (Fig. 7), suggesting LH_3 catalyzed the flow of electrons from NADH to molecular oxygen through the enzyme NADH dehydrogenase. However, in case of $Cu^{(II)}$-$(LH_2)_2$, formation of $O_2^{-\cdot}$ decreased considerably (Fig. 7). In these reactions, formation of superoxide ($O_2^{-\cdot}$) occurs when semiquinones are oxidized by molecular oxygen.[25-27] In the complex, the carbonyl at C_9 of LH_2^- is involved in coordinating Cu(II) leading to a substantial decrease in semiquinone formation. Only one carbonyl (C_{10}) on each LH_2^- is free to form semiquinones. Hence,

much less semiquinone formation is expected for the complex. Moreover, owing to the presence of Cu(II) in the complex, the semiquinone formed quickly transfers its electron to the metal centre leading to further decrease in its concentration.[54] This affects its interaction with molecular oxygen leading to decreased $O_2^{-\cdot}$ formation.

4. Conclusions

A mononuclear complex of Cu(II) with LH_3 [$Cu^{(II)}$-$(LH_2)_2$] was prepared and characterized by physico-chemical and spectroscopic studies. Although a single crystal was not obtained, the structure was solved from X-ray powder diffraction data that was corroborated by a DFT study. Ours is the first reported crystal structure of any hydroxy-9, 10-anthraquinone with a 3d-transition metal ion. Cyclic voltammetry of $Cu^{(II)}$-$(LH_2)_2$ in DMF showed one-electron reduction [$E_{1/2}$ = -0.810 V *vs.* Ag,AgCl/ KCl (saturated)] that occurred at the quinone moiety of the ligand. Findings from cyclic voltammetry was corroborated by predictions from a DFT study that suggested redox processes would be quinone based. Physicochemical and electrochemical attributes of purpurin and its Cu(II) complex were similar to the anthracycline drug doxorubicin and its Cu(II) complex. Interaction of the complex with CT DNA suggest while in case of purpurin binding constant values decreased with increase in pH, complex formation could prevent this trend. For the complex, binding with CT DNA not only increased but remained constant over a wide range of pH improving the latter's applicability. *In vitro* DNA topoiomerase relaxation assays showed [$Cu^{(II)}$-$(LH_2)_2$] was a dual poison for human DNA topoisomerase I and human DNA topoisomerase II enzymes like that known for CPT and DOX that was a significant improvement following complex formation. DNA cleavage assays for topoisomerase I and topoisomerase II in the presence of the complex and known ROS scavengers revealed DNA cleavage was due to stabilization of the enzyme-DNA adduct

and not due to ROS generation. With the help of ALL MOLT-4 cells, we could show that the complex inhibits topoisomerase I and topoisomerase II enzymes forming enzyme-DNA covalent complexes within the cells as revealed by the results of the immunoband depletion assay. The NADH dehydrogenase assay performed for determining ROS generation by the compounds revealed generation of superoxide radicals by $Cu^{(II)}$-$(LH_2)_2$ was much lower than LH_3.

Since the complex was found to be more potent in killing ALL MOLT-4 cells than LH_3 and considering findings on DNA topoisomerase enzymes it may be suggested that the complex targets topoisomerase I and topoisomerase II enzymes during anticancer activity. Findings from this study illustrate that $Cu^{(II)}$-$(LH_2)_2$ is a promising anticancer agent. Further understanding of the mode of action of the complex may rationally help to modify the chemical and biological properties to optimize anticancer activity.

Associated Content

Supporting Information

Physicochemical experiments on complex formation in solution. Spectroscopic characterization (IR, Mass, EPR) of the complex. Table showing TDDFT calculation. Various plots for evaluation of binding parameters of LH_3 and $Cu^{(II)}$-$(LH_2)_2$ with CT DNA. CIF and check CIF pdf files of $Cu^{(II)}$-$(LH_2)_2$.

Author Information

Corresponding Author

*Phone: +91-8902087756, Fax: +91-3324146223. E-mail: sdas@chemistry.jdvu.ac.in

Notes

The authors declare no competing financial interests.

Acknowledgements

Financial support from DST, Govt. of West Bengal [794(Sanc.)1(10) ST/P/S&T/9G-23/2013] in the form of a research project to S D is gratefully acknowledged. P D expresses his gratitude to the University Grants Commision, Government of India for a research fellowship. C K J also acknowledges University Grants Commision, Government of India for providing a research fellowship. S D offers his gratitude to Prof. Samita Basu, Head, CSD, SINP and former Head, Prof. Soumen Basak for allowing P D to carry out experiments on fluorescence and cyclic voltammetry. S D also wishes to thank Prof. Amitabha De and his student Ankan Dutta Chowdhury of CSD, SINP for their co-operation in carrying out cyclic voltammetry experiments.

Abbreviations:

LH_3: purpurin or 1,2,4-trihydroxy-9,10-anthraquinone, $Cu^{(II)}$-$(LH_2)_2$: Cu(II) complex of purpurin or LH_3, CT DNA: calf thymus DNA, ROS: reactive oxygen species, SOD: Superoxide dismutase, ETO: etoposide, CPT: camptothecin, DOX: doxorubicin, NAC: N-acetyl acetic acid, AA: Ascorbic acid.

References:

1. G. Minotti, P. Menna, E. Salvatorelli, G. Cairo, L. Gianni, *Pharmacol. Rev*., 2004, **56**, 185-229.
2. K. C. Chow, T. L. Macdonald, W. E. Ross, *Mol. Pharmacol*., 1988, **34**, 467-473.
3. J. C. Wang, *Nature Reviews, Molecular Cell Biology*, 2002, **3**, 430-440.
4. D. A. Koster, A. Crut, S. Shuman, M. Bjornsti, N. H. Dekker, ***Cell*** 2010, **142**, 519-530.
5. Y. Pommier, *Chem. Rev***.** 2009, **109**, 2894-2902.
6. Y. Pommier, *Curr. Med. Chem. Anti-cancer agent* 2004, **5**, 429-434.

7. Y. Pommier, E. Leo, H. L. Zhang, C. Marchand, *Chemistry & Biology* 2010, **17,** 421-433.

8. Y. Pommier, Nature Reviews, *Cancer* **2006,** 6, 789-802.

9. F. Arcamone, S. Penco in *Anthracycline and Anthracenedione-Based Anticancer Agents* (Ed. J. W. Lown), Elsevier, Amsterdam, **1988.**

10. A. J. M. Ferreri, E. Campo, A. Ambrosetti, F. Ilariucci, J. F. Seymour, R. Willemze, G. Arrigoni, G. Rossi, A. Lopez-Guillermo, E. Berti, M. Eriksson, M. Federico, S. Cortelazzo, S. Govi, N. Frungillo, S. Dell'Oro, M. Lestani, S. Asioli, E. Pedrinis, M. Ungari, T. Motta, R. Rossi, T. Artusi, P. Iuzzolino, E. Zucca, F. Cavalli, M. Ponzoni, *Ann. Oncol*. 2004, **15**, 1215-1221.

11. E. V. Barry, S. E. Lipshultz, S. E. Sallan, Anthracycline-induced cardiotoxicity: natural history, risk factors, and prevention, in *American Society of Clinical Oncology 2008 Educational Book* (Ed. R. Govindan), American Society of Clinical Oncology, Alexandria, 2008, pp. 448–453.

12. K. Schimmel, D. Richel, R. van den Brink, H. J. Guchelaar, *Cancer Treat. Rev*. 2004, **30**, 181-191.

13. M. I. Gharib, A. K. Burnett, *Eur. J. Heart. Fail.* 2002, **4**, 235-242.

14. L. C. M. Kremer, E. C.V. Dalen, M. Offringa, P. A. Voute, *Ann. Oncol*., 2002, **13**, 503-512.

15. S. M. Swain, F. S. Whaley, M. S. Ewer, *Cancer*, 2003, **97**, 2869-2879.

16. D. Iarussi, P. Indolfi, F. Casale, V. Martino,M. T. Di Tullio, R. Calabrò, *Paediatr. Drugs*, 2005, **7**, 67-76.

17. D. L. Keefe, *Semin. Oncol*., 2001, **28**, 2-7.

18. D. Cardinale, A. Colombo, G. Lamantia, N. Colombo, M. Civelli, G. D. Giacomi, M. Rubino, F. Veglia, C. Fiorentini, C. M. Cipolla, *J. Am. Col. Cardiol*., 55 (2010) 213-220.
19. J. L. Speyer, M. D. Green, A. Zeleniuch-Jacquotte, J. C. Wernz, M. Rey, J. Sanger, E. Kramer, V. Ferrans, H. Hochster, M. Meyers, *J. Clin. Oncol*., 1992, **10**, 117-127.
20. A. Moreno-Aspitia, E. A. Perez, *Clin. Ther.*, 2009, **31**, 1619-1640.
21. T. Pecere, M. V. Gazzola, C. Mucignat, C. Parolin, F. D.Vecchia, A. Cavaggioni, G. Basso, A. Diaspro, B. Salvato, M. Carli, G. Palù, *Cancer Res*. 2000, **60**, 2800-2804.
22. G. Cozza, M. Mazzorana, E. Papinutto, J. Bain, M. Elliott, G. di Maira, A. Gianoncelli, M. A. Pagano, S. Sarno, M. Ruzzene, R. Battistutta, F. Meggio, S. Moro, G. Zagotto, L. A. Pinna, *The Biochem. Jour*., 2009, **421**, 387-395.
23. P. Das, P. S. Guin, P. C. Mandal, M. Paul, S**.** Paul, S. Das, *J. Phy.Org. Chem***.,** 2011, **24**, 774-785.
24. P. S. Guin, S. Das, P. C. Mandal, *J. Phys. Org. Chem*., 2010, **23**, 477-482.
25. S. Das, A. Saha, P. C. Mandal, *Talanta*, 1996, **43**, 95-102.
26. M. M. L. Fialo, A. G. Suillerot, *Biochim. Biophys. Acta*, 1985, **840**, 91-98.
27. H. Beraldo, A. Garnier-Suillerot, L. Tosi, F. Lavelle, *Biochemistry*, 1985, **24**, 284-289.
28. C. Santini, M. Pellei, V. Gandin, M. Porchia, F. Tisato, C, Marzano, *Chemical Reviews*, 2014, 114, 815-862.
29. A. Kheirolomoom, L. M. Mahakian, C. Y. Lai, H. A. Lindfors, J. W. Seo, E. E. Paoli, K. D. Watson, E. M. Haynam, E. S. Ingham, L. Xing, R. H. Cheng, A. D. Borowsky, R. D. Cardiff, K. W. Ferrara, *Mol Pharm*., 2010, **7**, 1948-1958.
30. M. D. Vaira, P. Orioli, F. Piccioli, B. Bruni, L. Messori, *Inorg. Chem*., 2003, **42**, 3157-3159.

31. D. Cova, M. Sassano, E. Monti, F. Piccinini, *Archives of Toxicology*, 1990, **64**, 597-598.

32. P. S. Guin, S. Das, P. C. Mandal, *J. Inorg. Biochem*., 2009, **103**, 1702-1710.

33. Solvent extraction in Textbook of Quantitative Chemical analysis (Eds. G.H. Jeffery, J. Bassett, J. Mendham, R.C. Denney), fifth ed., ELBS/Longman, Great Britain, 1989, pp 178-184.

34. A. Altomare, C. Giacovazzo, A. Guagliardi, A. G. G. Moliterni, R. Rizzi, P. E. Werner, *J. App. Cryst*., 2000, **33**, 1180-1186.

35. V. Favre-Nicolin, R. Cerny, *J. App. Cryst*., 2002, **35**, 734. http:// objcryst.sourceforge.net.

36. J. J. P. Stewart, MOPAC 5.0, A general purpose Molecular Orbital Package (QCEP 455).

37. A. C. Larson, R. B. Von Dreele, General Structure Analysis System (GSAS), Los Alamos National Laboratory Report LAUR (2000) 86-748.

38. B. H. Toby, *J. App. Cryst*., 2001, **34**, 210-213.

39. A. D. Becke, *J. Chem. Phys*., 1993, **98**, 5648-5652.

40. C. Lee, W. Yang, R. G. Parr, *Phys. Rev. B*, 1988, **37**, 785-789.

41. M. J. Frisch, G. W. Trucks, H. B. Schlegel, G. E. Scuseria, M. A. Robb, J. R. Cheeseman, G. Scalmani, V. Barone, B. Mennucci, G. A. Petersson, H. Nakatsuji, M. Caricato, X. Li, H. P. Hratchian, A. F. Izmaylov, J. Bloino, G. Zheng, J. L. Sonnenberg, M. Hada, M. Ehara, K. Toyota, R. Fukuda, J. Hasegawa, M. Ishida, T. Nakajima, Y. Honda, O. Kitao, H. Nakai, T. Vreven, J. A. Montgomery, Jr., J. E. Peralta, F. Ogliaro, M. Bearpark, J. J. Heyd, E. Brothers, K. N. Kudin, V. N. Staroverov, R. Kobayashi, J. Normand, K. Raghavachari, A. Rendell, J. C. Burant, S. S. Iyengar, J. Tomasi, M. Cossi, N. Rega, J. M. Millam, M. Klene, J. E. Knox, J. B.

Cross, V. Bakken, C. Adamo, J. Jaramillo, R. Gomperts, R. E. Stratmann, O. Yazyev, A. J. Austin, R. Cammi, C. Pomelli, J. W. Ochterski, R. L. Martin, K. Morokuma, V. G. Zakrzewski, G. A. Voth, P. Salvador, J. J. Dannenberg, S. Dapprich, A. D. Daniels, O. Farkas, J. B. Foresman, J. V. Ortiz, J. Cioslowski, D. J. Fox, Gaussian 09 (Revision A.02): Gaussian, Inc.: Wallingford CT 2009.

42. T. H. Dunning Jr., P. J. Hay, in Modern Theoretical Chemistry (Ed. H. F. Schaefer), III, New York, 1976, pp 1-28.
43. P. J. Hay, W. R. Wadt, *J. Chem. Phys*., 1985, **82**, 299-310.
44. N. M. O'Boyle, GaussSum 2.1 (2007) available at http://gausssum.sf.net.
45. N. M. O'Boyle, A. L. Tenderhol, K. M. Langner, *J. Comp. Chem*., 2008, **29**, 839-845.
46. E. D. Glendening, A. E. Reed, J. E. Carpenter, F. Weinhold, NBO, version 3.1, Theoretical Chemistry Institute, University of Wisconsin: Madison, WI (2001).
47. A. E. Reed, F. Weinhold, *J. Chem. Phys*., 1985, **83**, 1736-1740.
48. A. E. Reed, L. A. Curtiss, F. Weinhold, *Chem. Rev*., 1988, **88**, 899-926.
49. F. Weinhold, in Natural Bond Orbital Methods in Encyclopedia of Computational Chemistry (Ed. P. V. R. Schleyer), Wiley, UK, 1998, pp 1792-1811.
50. D. A. Zhurko, G. A. Zhurko, ChemCraft 1.5; Plimus: San Diego, CA, 92130, http://www.chemcraftprog.com.
51. S. Roy, R. Banerjee, M. Sarkar, *J. Inorg. Biochem*., 2006, **100**, 1320-1331.
52. S. Chakraborti, B. Bhattacharyya, D. Dasgupta, *J. Phys. Chem. B*, 2002, **106**, 6947-6953.
53. H.R. Mahler, in Methods in Enzymology 11 (Eds. S. P. Colowick, N. O. Kaplan), Academic Press, New York, 1955, pp 668-672.
54. S. Das, A. Bhattacharya, P. C. Mandal, M. C. Rath, T. Mukherjee, *Rad. Phy.Chem*., 2002, **65**, 93-100.

55. J. E. B. Randles, *Trans. Faraday Soc*., 1948, **44**, 322-327.

56. *Electrochemical Methods Fundamental and Applications*, A. J. Bard, L. R. Faulkner, 2nd ed., John Wiley & Sons. New York, 2001.

57. R. S. Nicholson, *Anal. Chem*., 1966, **38,** 1406.

58. S. Mukherjee, P. Das, S. Das, *J. Phy. Org. Chem*., 2012, **25**, 385-393.

59. F. Frezard, Garnier-Suillerot, *Biochim. Biophy. Acta*, 1990, **1036**, 121-127.

60. S. Mukherjee, P. Gopal, S. Paul, S. Das, *J. Anal. Oncol*., 2014, **3**.

61. H. A. Benesi, J. H. Hildebrand, *J. Am. Chem. Soc*. 1949, **71**, 2703-2707.

62. G. Scatchard, *Ann. N. Y. Acad. Sci*., 1949, **51**, 660-672.

63. S. M. Attia, *Arch. Toxicol*., 2012, **86**, 725-731.

64. S. Belin, F. Kaya, G. Duisit, S. Giacometti, J. Ciccolini, M. Fonte´s, *PLoS ONE*, 2009, **4(2)**, e4409. doi:10.1371/journal.pone.0004409.

Figure Legends

Figure 1. a) Final Rietveld plot, where red curve denotes experimental pattern, green curve denotes the simulated pattern and pink curve indicates the difference of these two patterns. **b)** ORTEP diagram of the complex $Cu^{(II)}$-$(LH_2)_2$ (for clarity guest water molecules were omitted). Ellipsoids are drawn at 30% probability. **c)** DFT optimized structure of $Cu^{(II)}$-$(LH_2)_2$ complex. **d)** to **g)** are pictorial representation of respective MO diagrams of $Cu^{(II)}$-$(LH_2)_2$ complex. **h)** Spin density plot of $Cu^{(II)}$-$(LH_2)_2$ complex.

Figure 2. a) Cyclic voltammogram of 120 μM of $Cu^{(II)}$-$(LH_2)_2$ solution in DMF recorded at 0.1 V/s potential sweep rate in 0.1M TBAB as supporting electrolyte, using glassy carbon electrode (0.1256 cm^2) at 298K. **b)** Linear dependence of cathodic peak current on square root of potential sweep rate for one step two electron reduction of $Cu^{(II)}$-$(LH_2)_2$ in DMF.

Figure 3. a) and b) Dependence of intrinsic binding constants (K*) for LH_3 interacting with CT DNA for a variation of pH in the medium. An average of all K* values was considered for this plot. Solid line is the fitted data that obeys equation 8 [Fig. 3a)] & equation 9 [Fig. 3b)]. [LH_3] = 75 μM; [NaCl] = 120 mM; [Tris buffer] = 15 mM; T = 298 K. **c)** Absorbance spectrum showing interaction of $Cu^{(II)}$-$(LH_2)_2$ with CT DNA in the absence (1) and presence (2) 296.83 μM, (3) 720.8729 μM, (4) 1218.027 μM, (5) 1682.03 μM, (6) 1974.56 μM, (7) 2523.05 μM, (8) 3027.66 μM, (9) 3493.46 μM of CT DNA. **d)** Binding isotherm for the spectrophotometric study of $Cu^{(II)}$-$(LH_2)_2$ with CT DNA and the corresponding non-linear fit. Inset, the mole ratio plot of the same; **e)** Fluorescence spectrum of $Cu^{(II)}$-$(LH_2)_2$ interacting with CT DNA in absence (1) and presence (2) 15.50 μM, (3) 30.95 μM, (4) 77.14 μM, (5) 153.53 μM, (6) 304.04 μM, (7) 667.71 μM, (8) 1722.87 μM, (9) 2584.3 μM of CT DNA. **f)** Binding isotherm of fluorometric study of $Cu^{(II)}$-$(LH_2)_2$ with CT DNA and the corresponding non-linear fit. Inset, the mole ratio plot of the same; [$Cu^{(II)}$-$(LH_2)_2$] = 75 μM, [NaCl] = 120 mM; [Tris buffer] = 15 mM of pH 7.42; T = 298 K.

Figure 4. DNA Topoisomerase relaxation assays. **a)** DNA topo I relaxation assay. Lane 1 is 100 fmol supercoiled pBS (SK^+) DNA, lane 2 is 100 fmol supercoiled pBS (SK^+) DNA with 40 μM LH_3, lane 3 is 100 fmol supercoiled pBS (SK^+) DNA with 40 μM $Cu^{(II)}$-$(LH_2)_2$, lane 4 is 100 fmol supercoiled pBS (SK^+) DNA with 50 fmol topoisomerase I enzyme, lane 5 is same as lane 4 but with 10 μM CPT, lane 6 is same as lane 4 but with 20 μM LH_3, lane 7 is same as lane 4 but with 40 μM LH_3. Lane 8 is same as lane 4 but with 10 μM $Cu^{(II)}$-$(LH_2)_2$, lane 9 is same as lane 4 but with 20 μM $Cu^{(II)}$-$(LH_2)_2$. All the reactions were incubated at 37 ^oC for 30 minutes and analysed by agarose gel electrophoresis. **b)** DNA topo II relaxation assay. Lane 1 is 100 fmol supercoiled pBS (SK^+) DNA, lane 2 is 100 fmol supercoiled pBS (SK^+) DNA with 40 μM LH_3, lane 3 is 100 fmol supercoiled pBS (SK^+) DNA with 40 μM $Cu^{(II)}$-$(LH_2)_2$, lane 4 is 100 fmol supercoiled pBS (SK^+) DNA with 50 fmol topoisomerase II enzyme, lane 5 is same as lane 4 but with 10 μM DOX, lane 6 is same as lane 4 but with 20 μM LH_3, lane 7 is same as lane 4 but with 40 μM LH_3. Lane 8 is same as lane 4 but with 10 μM $Cu^{(II)}$-$(LH_2)_2$, lane 9 is same as lane 4 but with 20 μM $Cu^{(II)}$-

$(LH_2)_2$. All the reactions were incubated at 37 ^oC for 30 minutes and analysed by agarose gel electrophoresis.

Figure 5: Plasmid cleavage assays**. a)** DNA Topoisomerase I plasmid cleavage assay. All the cleavage assays were performed in the presence of NAC and ascorbic acid. Lane 1 is 100 fmol supercoiled pBS (SK^+) DNA, lane 2 is 100 fmol supercoiled pBS (SK^+) DNA with 40 μM LH_3, lane 3 is 100 fmol supercoiled pBS (SK^+) DNA with 40 μM $Cu^{(II)}$-$(LH_2)_2$, lane 4 is 100 fmol supercoiled pBS (SK^+) DNA with 500 fmol topoisomerase I enzyme, lane 5 is same as lane 4 but with 10 μM CPT, lane 6 is same as lane 4 but with 20 μM LH_3, lane 7 is same as lane 4 but with 40 μM LH_3. Lane 8 is same as lane 4 but with 10 μM $Cu^{(II)}$-$(LH_2)_2$, lane 9 is same as lane 4 but with 20 μM $Cu^{(II)}$-$(LH_2)_2$. All the reactions were incubated at 37 ^oC for 30 minutes and stopped with 0.5% SDS. The enzyme was digested by proteinase K treatment and reactions were analysed by agarose gel electrophoresis. **b)** DNA Topoisomerase II plasmid cleavage assay. Lane 1 is 100 fmol supercoiled pBS (SK^+) DNA, lane 2 is 100 fmol supercoiled pBS (SK^+) DNA with 40 μM LH_3, lane 3 is 100 fmol supercoiled pBS (SK^+) DNA with 40 μM $Cu^{(II)}$-$(LH_2)_2$, lane 4 is 100 fmol supercoiled pBS (SK^+) DNA with 500 fmol topoisomerase II enzyme, lane 5 is same as lane 4 but with 10 μM DOX, lane 6 is same as lane 4 but with 20 μM LH_3, lane 7 is same as lane 4 but with 40 μM LH_3. Lane 8 is same as lane 4 but with 10 μM $Cu^{(II)}$-$(LH_2)_2$, lane 9 is same as lane 4 but with 20 μM $Cu^{(II)}$-$(LH_2)_2$. All the reactions were incubated at 37 ^oC for 30 minutes and stopped with 0.5% SDS. The enzyme was digested by proteinase K treatment and reactions were analysed by agarose gel electrophoresis.

Figure 6. **a)** Plot showing effects of CPT, ETO and DOX on MOLT-4 cells. **b)** Dose response curve for effects of LH_3 and $Cu^{(II)}$-$(LH_2)_2$ on MOLT-4 cells. In both cases, MOLT-4 cells were treated with respective compounds for 72 hours and MTT assay was performed. **c)** Immuno band depletion assay. Cultured MOLT-4 Cells were treated with indicated concentrations of the compounds and harvested at 0 hour, 4 hours, 8 hours and 12 hours post treatment. CPT (10 μM) and DOX (10 μM) were used as positive controls.

Figure 7. Effect of LH_3 and $Cu^{(II)}$-$(LH_2)_2$ on superoxide formation by NADH dehydrogenase determined spectrophotometrically by the rate of SOD-inhibitable cytochrome-c reduction at pH 7.4 Tris buffer; [SOD] = 40 μg/mL; [NADH] = 160 μM; [Cytochrome c] = 80 μM; [NADH dehydrogenase] = 5 UL^{-1}.

Tables

Table 1: Crystallographic data and refinement parameters obtained from PXRD data analysis.

Formula	C_{28} H_{10} Cu O_{12}
Formula Weight	601.92
Crystal System	Triclinic
Space group	P -1
a/Å	12.6644(14)
b/Å	12.2799(10)
c /Å	10.4602(13)
α/°	97.155(11)
β/°	113.937(9)
γ /°	61.539(6)
V /$Å^3$	1302.34(18)
Z	2
ρ_{calc} /g cm^{-3}	1.494
Temperature /K	293
Radiation /Å	1.54184
2θ range/°	5 - 80
R_{wp}	0.0685
R_p	0.0429

Table 2: Selected bond lengths and bond angles of $Cu^{(II)}$-$(LH_2)_2$ obtained by refinement of the PXRD pattern and those calculated by DFT method

Bonds	Bond lengths (Å)	
	Obtained by refinement of the PXRD pattern	Calculated by DFT method
Cu1-O18	1.8469	1.919
Cu1-O19	1.8839	1.954
Cu1-O34	1.8843	1.954
Cu1-O35	1.8467	1.919
	Bond angles (°)	
O18 -Cu1 -O19	92.89	90.02
O18 -Cu1 -O34	87.23	89.98
O18 -Cu1 -O35	179.88	179.98
O19 -Cu1 -O34	179.86	179.99
O19 -Cu1 -O35	87.00	89.98
O34 -Cu1 -O35	92.89	90.02
Cu1 -O18 -C5	126.23	127.75
Cu1 -O19 -C10	129.45	131.05
Cu1 -O34 -C22	129.44	131.05
Cu1 -O35 -C26	126.25	127.75

Table 3. TDDFT table of $Cu^{(II)}$-$(LH_2)_2$ complex.

Energy (eV)	Wavelength (nm)	*f*	Involved transition	character
2.4741	501.13	0.3618	α HOMO-1→α LUMO (0.57671)	Ligand (pπ) → Ligand (pπ*)
3.2292	383.94	0.5022	β -HOMO-6 → β-LUMO (0.70551)	Ligand (pπ) → Ligand (pπ*)

Table 4. Electrochemical properties of single step one-electron reduction of $Cu^{(II)}$-$(LH_2)_2$ in DMF.

ν (V/s)	i_{pa}/i_{pc}	$-E_{1/2}$ (V)
0.025	1.0500	0.817
0.050	1.0175	0.812
0.075	1.0283	0.804
0.100	1.1208	0.801
0.200	1.0536	0.805
0.300	1.0339	0.819
0.400	1.0641	0.809
0.500	1.0768	0.820
0.750	1.0414	0.818
1.000	1.0233	0.826

Table 5. Results of the binding parameters of $Cu^{(II)}$-$(LH_2)_2$ with CT DNA by spectroscopic techniques.

Experiment	$K_{app}\times10^{-3}$ (M^{-1}) from double-reciprocal plot	$K_{app}\times10^{-3}$ (M^{-1}) from non-linear curve fitting	$K'\times10^{-4}$ (M^{-1}) = K_{app} x n_b	$K'\times10^{-4}$ (M^{-1}) Scatchard plot	$K'\times10^{-4}$ (M^{-1}) Benesi-Hildebrand double-reciprocal plot	n_b Scatchard plot
UV-Vis	3.55 ± 0.42	1.72 ± 0.50	3.84 ± 0.15	4.80 ± 0.20	1.60 ± 0.20	10.82 ± 0.20
Fluorimetry	5.23 ± 0.22	6.28 ± 0.30	4.49 ± 0.28	4.04 ± 0.33	—	8.58 ± 0.48

Figures

Fig. 1

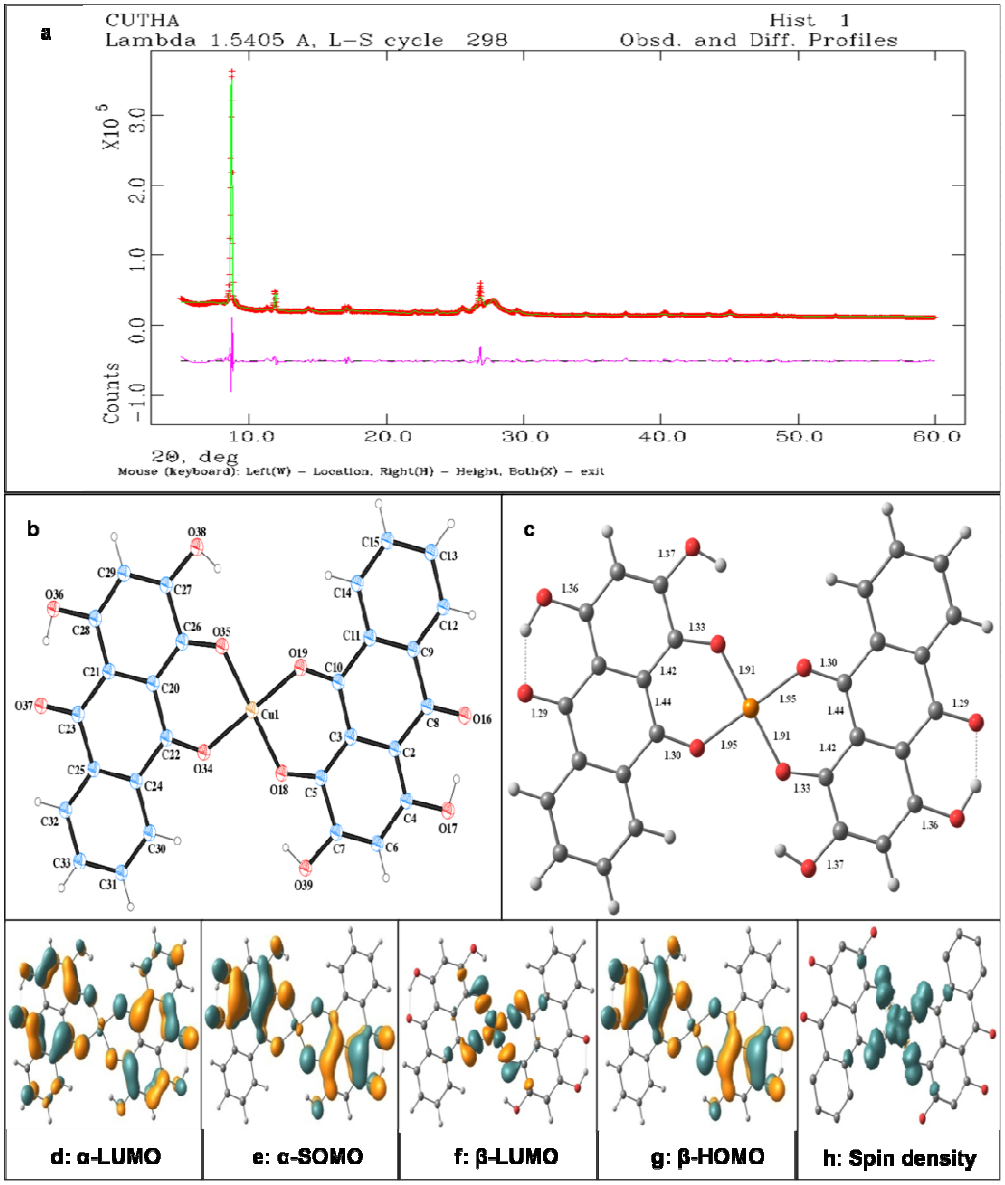

Fig. 2

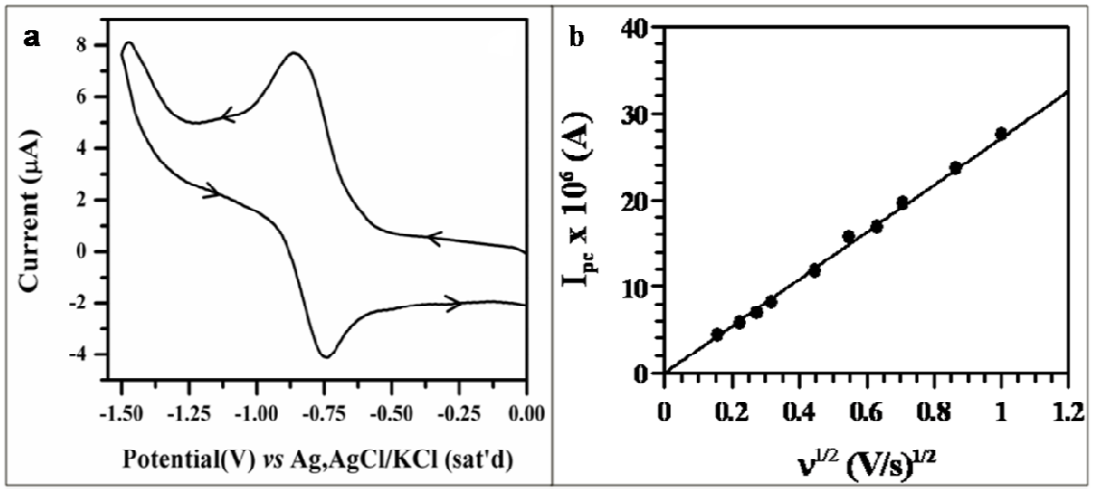

Fig. 3

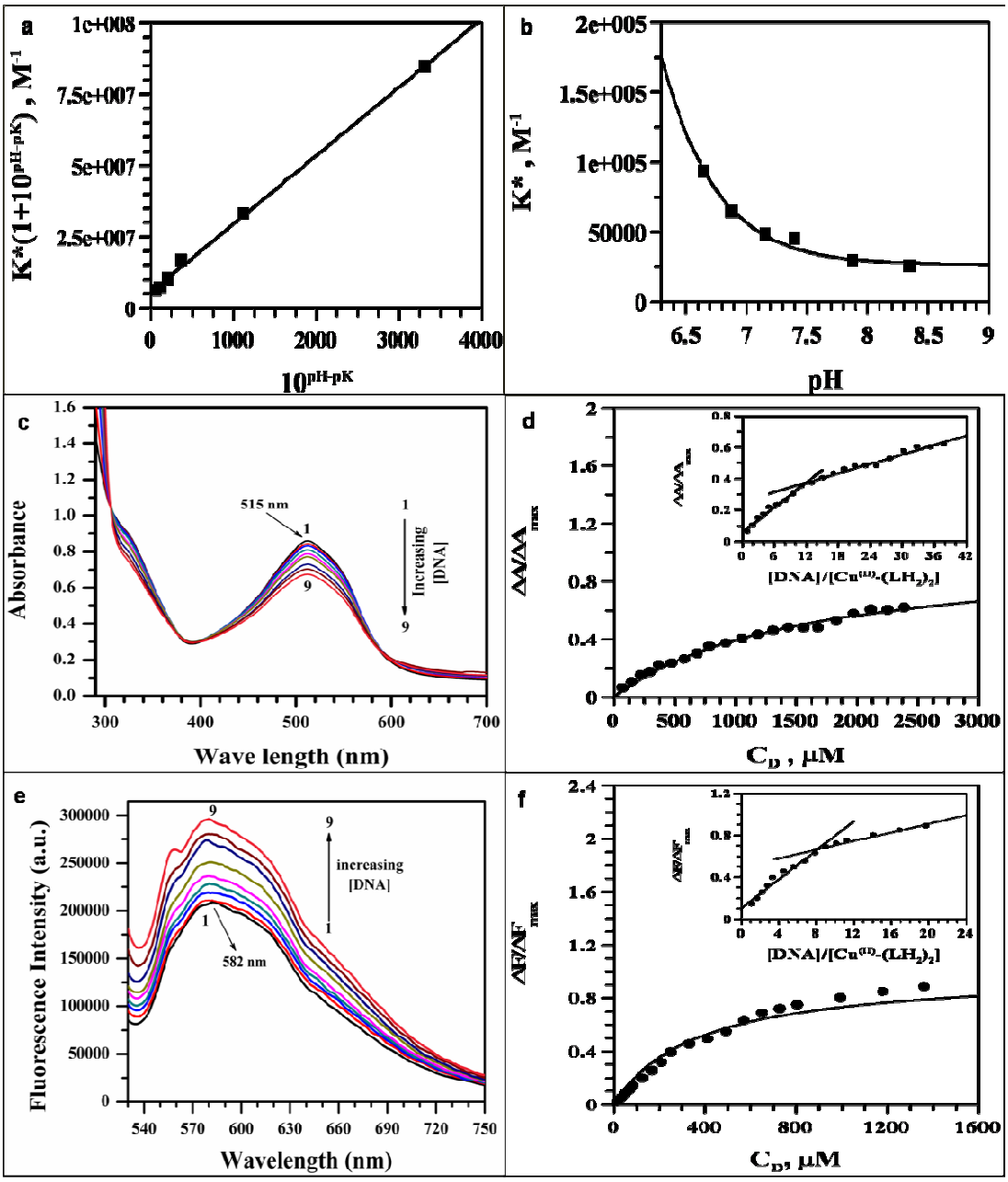

Fig. 4

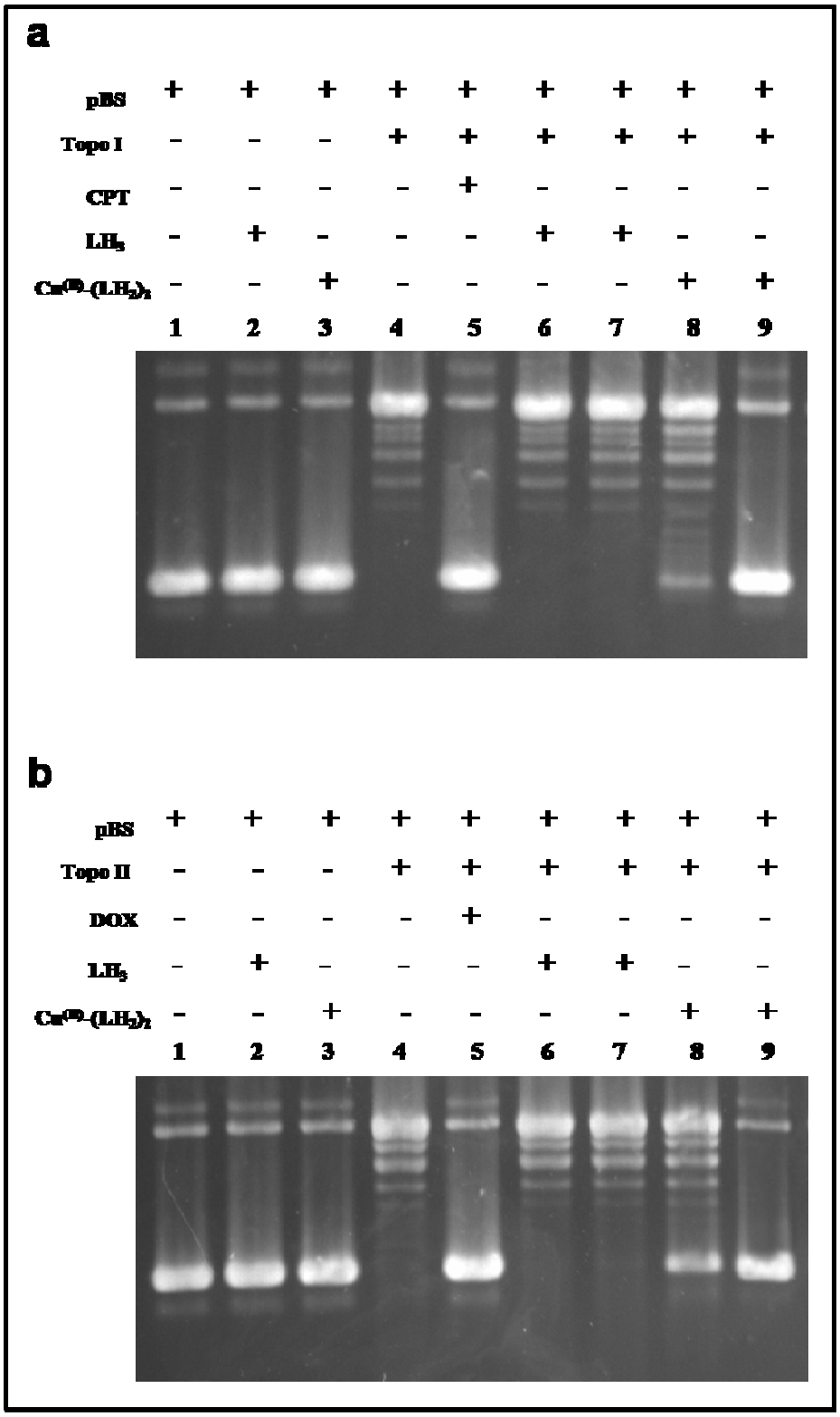

Fig. 5

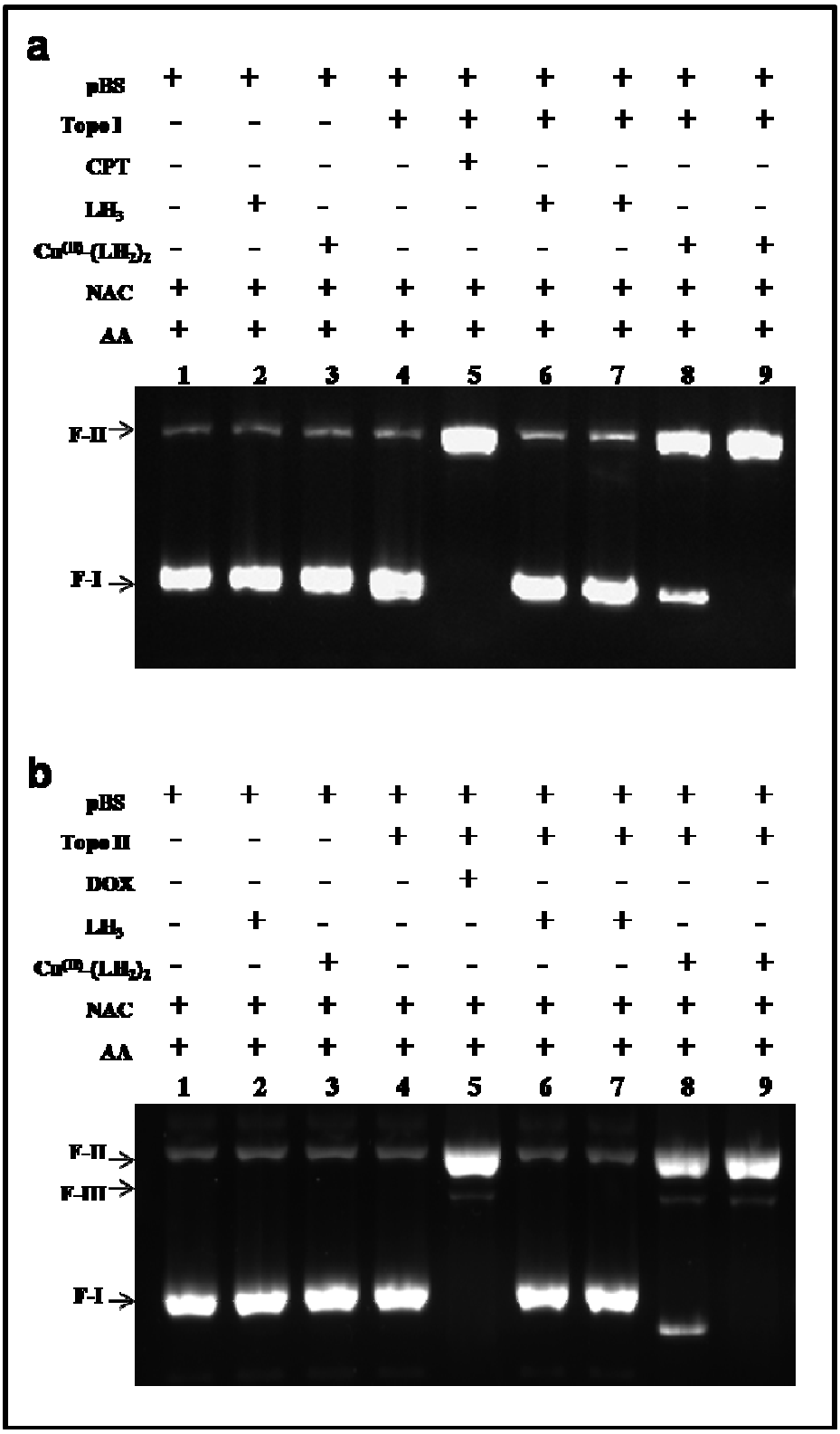

Fig. 6

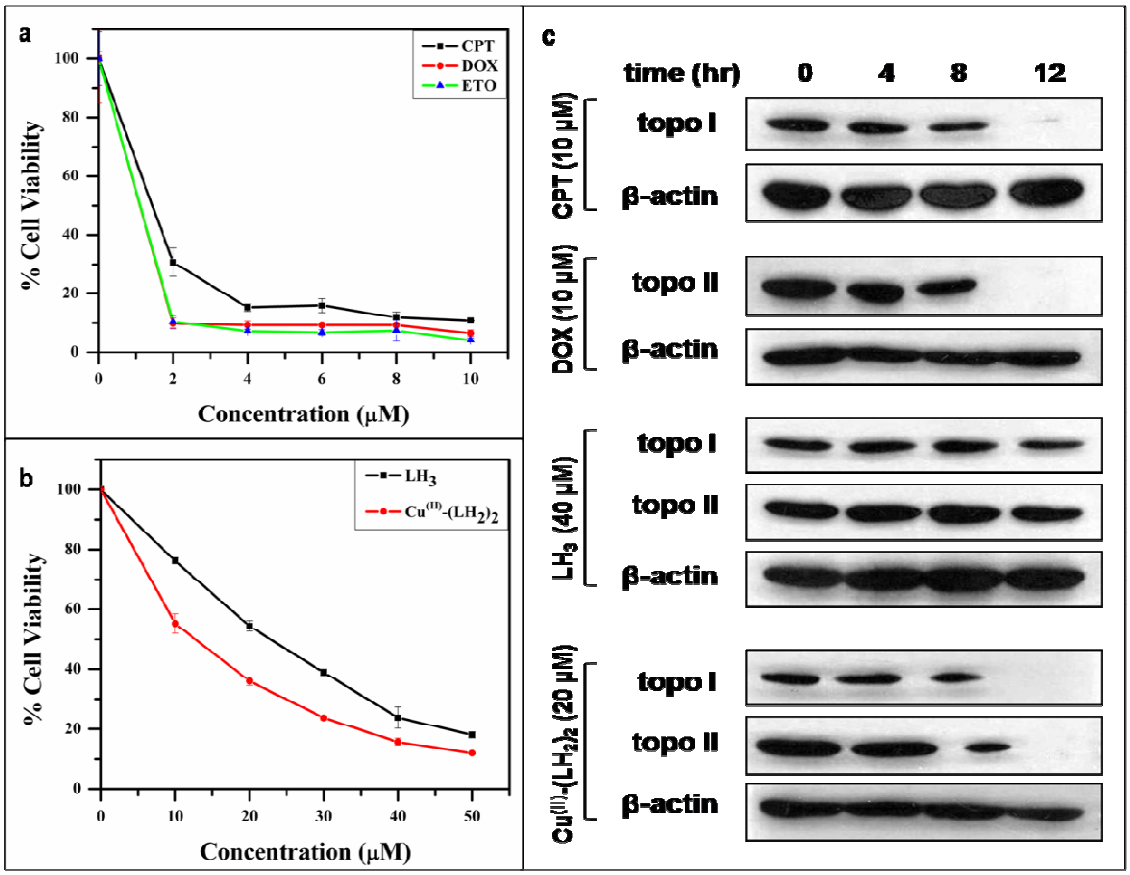

Fig. 7